Texas Instruments

ISSUE 2, 2025

Analog Design JOURNAL

Table of contents

2H2025

Choosing a position sensor in motor control

Introduction

Are there still position sensors in motors, since the trend is to go “sensorless”? The full answer to this question is rather convoluted, but basically, position sensors are here to stay. There are applications such as power tools where a sensorless design with a brushless-DC motor block commutation or a field-oriented-control (FOC) brushless-AC motor works without any rotary angle sensor. But the reality is that end equipment such as industrial and humanoid robots, autonomous mobile robots, and linear motor transport systems absolutely need rotary angle or linear position sensors.

Using a position sensor with brushless motor control

Position sensors are not just used for the commutation of stator currents with brushless-DC or brushless-AC motors, but also for speed and position control. Industrial multiaxis robots often include a gear between the motor shaft and robot axis. A rotary angle sensor coupled with the motor shaft not only needs to sense the rotor angle, but also count the turns of the motor shaft to control the equivalent absolute angle position of the corresponding robot axis. Depending on the application, the type of encoder will vary.

Incremental and absolute encoders

Incremental encoders typically use ABZ digital or analog unidirectional interfaces, where two quadrature-encoded digital pulse train signals (A and B) or two analog Sin/Cos signals (A and B), allow for a low latency relative angle measurement with high resolution from approximately 10 bits up to 28 bits. An optional index (Z or I) enables absolute mechanical angle information. Incremental encoders do not provide an absolute angle at startup, and need to turn up to one revolution before the index occurs. Therefore, these encoders fit well in speed-variable applications that need very low latency (<1µs) but do not need an absolute angle at startup.

Conversely, absolute single- or multiturn rotary encoders offer an absolute angle position at startup. They offer a bidirectional **RS-485** interface with vendor-specific protocols, and enable time-triggered angle measurement as well as information such as rotary speed and number of rotary turns. The angle resolution typically goes from 10 bits to >30 bits, with a latency as low as 10µs to meet a wide range of industrial applications. The position resolution is typically the data format, which transmits through the digital interface. For example, an angle with a 20-bit integer format has a resolution of $360/2^{20}$; 0h = 0 degrees and 0xFFFFF = 360 degrees-$360/2^{20}$. Overall system noise is significantly higher than quantization noise; the effective number of bits (ENOB) characterizes this effect.

Equation 1 calculates the ENOB of the angle with the standard deviation of the angle measured in degree:

$$\text{ENOB [bit]} = (20 \cdot \log10(360/\text{stdev(angle)}) - 1.76)/6.02 \quad (1)$$

The root mean square of the angle noise signal equals the standard deviation (1 sigma). **Figure 1** illustrates the angle accuracy; the related angular error is larger than the standard deviation. The angle accuracy not only depends on the peak noise, which often uses the 6-sigma value, but also the nonlinearity over one revolution.

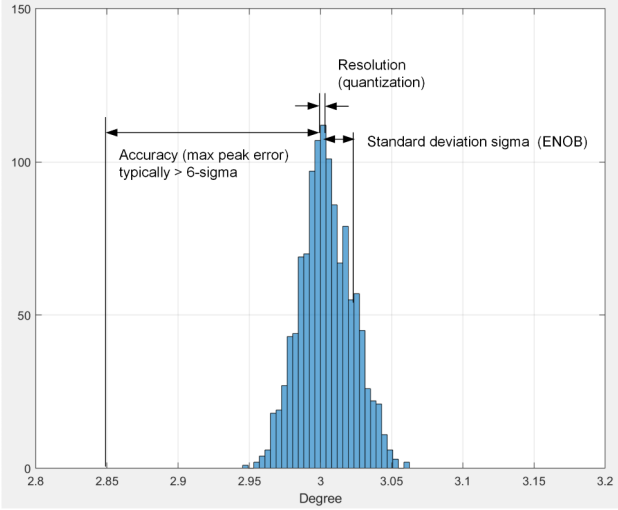

Figure 1. *Static angle distribution.*

FOC motor-control techniques and requirements for encoders

The FOC method shown in **Figure 2** is a high-performance technique that controls the resulting stator current vector according to the rotor magnetic flux angle to maximize torque with permanent-magnet synchronous motors. FOC enables smooth torque with fast transient response from standstill to high-speed operation. Accurate and low-latency measurement of the rotor magnet field angle will decompose the three stator-phase currents (i_U, i_V and i_W) into a rotor magnetic field-oriented coordinate system, with i_q equal to the torque-generating current and i_d equal to the field-weakening current.

In end equipment such as humanoid robots, the absolute rotary angle is typically measured at an accuracy from 1 degree to 0.1 degrees, an ENOB from 12 bits to 15 bits, and sample rates from 8kHz to 32kHz. The rotary angle is sensed simultaneously with the motor-phase currents. A low-latency angle measurement of <20µs enables enough time for the microcontroller (MCU) to run the control algorithms and update the pulse-width modulator (PWM) for the next PWM cycle.

It is possible to integrate rotary angle sensors into the motor housing, as in most humanoid robots, or in separate housing for mounting onto the motor shaft. Both cases require operation at high temperatures – often up to 125C ambient. In humanoid robots, where the control MCU is located close to the rotary encoder, 360-degree angle sensors such as TI's TMAG6180-Q1 anisotropic magnetoresistive (AMR) sensor offer a cost-efficient and low-latency interface.

Unlike rotary motors, linear motor-based transport systems require absolute linear position sensing, but still apply FOC for maximum torque. A 12-bit position resolution with <100µs latency is often sufficient.

In addition, achieving International Electrotechnical Commission 62061 or International Organization for Standardization (ISO) 13849 functional safety in industrial machinery requires safety-certified encoders determined by the safety integrity level or performance level, as well as additional diagnostics with the position sensor to detect random hardware faults. In automotive applications, systems designed according to ISO 26262 run diagnostics during system startup, whereas industrial systems require continuous diagnostics during normal operation, since they often run 24/7.

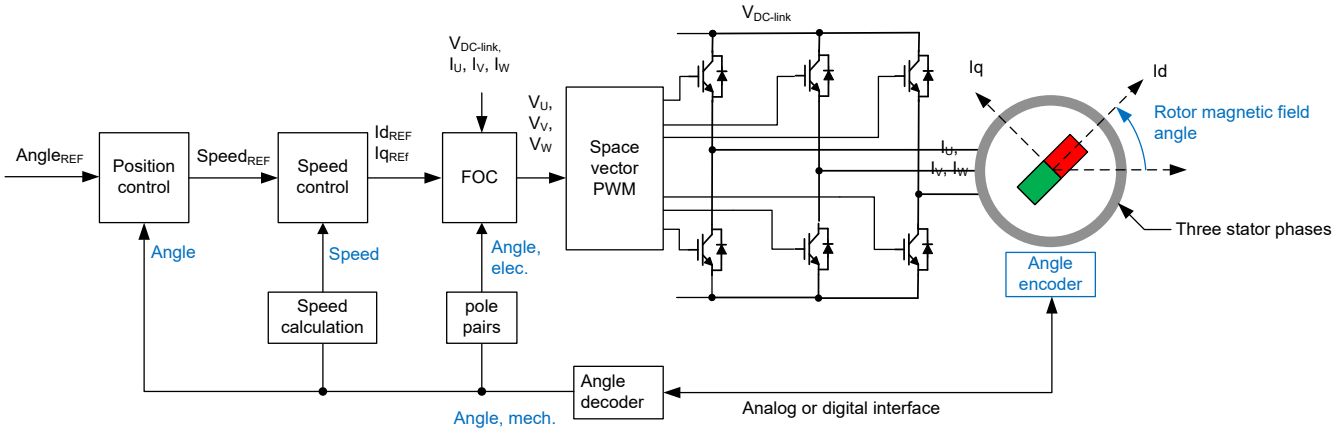

Figure 2. *Cascaded position, speed and FOC.*

Position sensor technologies

The predominant types of position sensors are optical, magnetic, inductive or capacitive. Optical sensors typically offer the highest resolution (although magnetic and inductive sensors are more reliable), and may offer a lower total system cost. In industrial or automotive systems, large current flows in nearby wiring necessitate a sensor technology such as inductive that is immune to magnetic stray fields. Capacitive sensors typically have lower resolution than inductive and magnetic sensors and are not as common.

For cost-sensitive systems in harsh environments (for example, high temperatures caused by motor integration), TI offers magnetic and inductive position sensors.

Magnetic position sensors

Magnetic encoders enable a cost-efficient method to detect rotary or linear movement while providing immunity in harsh environments that may include dust, oil and water. Magnetic position sensors detect magnetic field changes, convert them into electrical signals, and generate output signals. There are a variety of magnetic position sensor technologies, including Hall-effect, AMR, tunneling magnetoresistance (TMR) and giant magnetoresistance (GMR). **Table 1** lists each sensor's benefits and drawbacks.

Parameter	Hall Effect (without a magnetic flux concentrator)	Hall Effect (with a magnetic flux concentrator)	AMR	GMR	TMR
Operation region	–	–	Saturation	Saturation	Saturation
Cost	Least expensive	>Hall	>Hall	>Hall and AMR	Most expensive
Angles measured	XYZ	XYZ	XY	XY	XY
Angle range (degrees)	0-360	0-360	0-180 (the TMAG6180-Q1 extends to 360)	0-360	0-360
Latency	High	High	Low	Low	Low
Angle error (degrees)	<1.2 **1**	<1 **1**	<0.6 **1**	>1 **2**	<0.6 **2**
Magnetic flux density range (limits magnetic air-gap distances) (in milliTeslas)	0-300	0-70	>20-unlimited (the TMAG6180-Q1 tolerates up to 1,000)	20-120	20-120

Table 1. *Comparison of magnetic sensor technologies: Key features and specs.*

1. After gain and offset calibration.
2. After gain, offset and orthogonality calibration

Linear position example with a 3D Hall-effect linear sensor

In linear motor transport systems with fast-moving payload carriers zipping by at 5m/s to 15 m/s, a 12-bit position resolution with latency <100µs and sample rates ≤8kHz is often sufficient, while multiple position sensors connect to a single MCU through a high-speed Serial Peripheral Interface (SPI) bus, as shown in **Figure 3**.

The **TMAG5170** 3D Hall-effect sensor provides three main advantages – accuracy, low latency and board placement flexibility. The sensitivity error drift across the full temperature range is less than 2.8%. A 10MHz SPI enables low latency. Additionally, onboard 3D sensing elements enable configurable XY, YZ or XZ sensing directions, enhancing flexibility when placing the sensor in relation to the magnet.

The **Accurate Low-Latency Linear Position Sense Reference Design with Quad 3D Hall-Effect Sensors** uses the **TMAG5170** placed at 25mm intervals for precise, low-latency linear position sensing. A C2000™ MCU reads out the magnetic Z and X field data from all four TMAG5170 sensors for sample rates ≥8kHz, and calculates the moving magnet position with an error <0.15mm and latency <57.5µs.

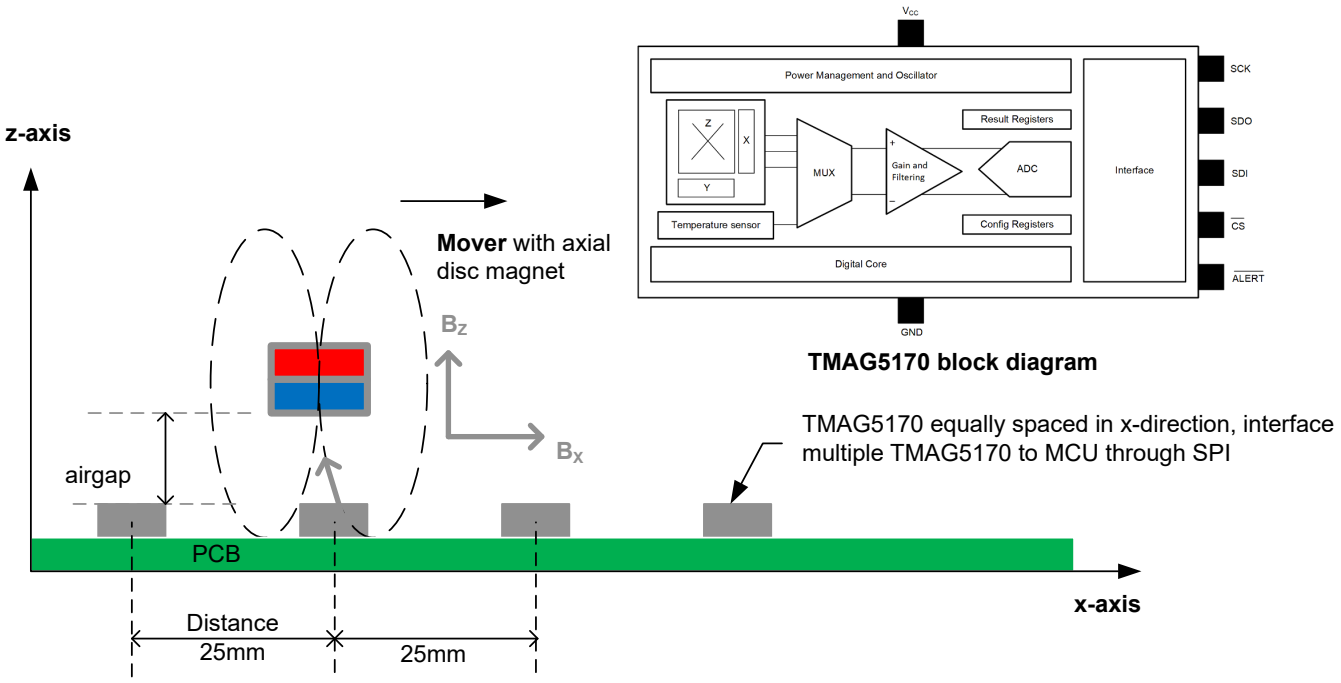

Figure 3. *The TMAG5170 in a linear motor transport system.*

Rotary angle example with an AMR sensor

The AMR sensor comprises four magnetoresistance Wheatstone bridges, where the voltage differences of two bridges' output terminals will reflect the external magnetic field magnitude.

Compared to Hall-effect sensors, AMR sensors have higher frequency operation and a higher signal-to-noise ratio (SNR). Compared to GMR and TMR sensors, AMR sensors have a relatively negligible orthogonality error. In applications such as servo drives that need a high-accuracy encoder, AMR sensors are often preferable given their higher magnetic field tolerance, yielding overall better immunity.

The **TMAG6180-Q1** 2D AMR angle sensor measures magnetic fields and produces two differential (or single-ended) voltage outputs proportional to those magnetic fields. The <2µs latency of the TMAG6180-Q1 also

minimizes angle errors caused by high-speed movement. Integrated Hall-effect switches produce two digital quadrant outputs (Q0 and Q1), thus extending the angle detection range to 360 degrees. Together with the sine and cosine waveforms, the Q0 and Q1 digital outputs are enough to determine the absolute rotary angle. **Figure 4** is a functional block diagram of the TMAG6180-Q1, while **Figure 5** shows the output waveforms.

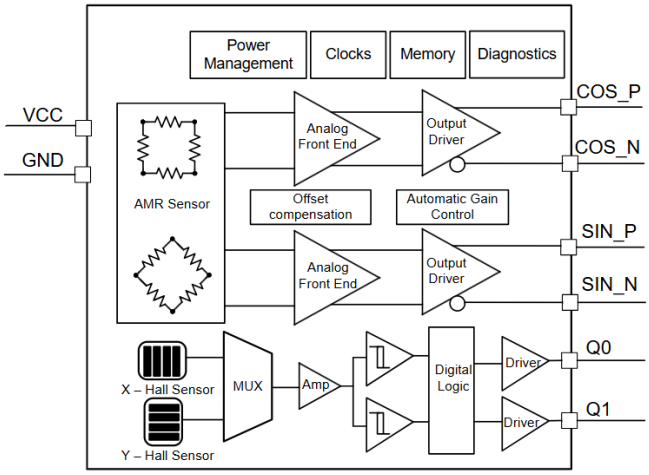

Figure 4. *TMAG6180-Q1 block diagram.*

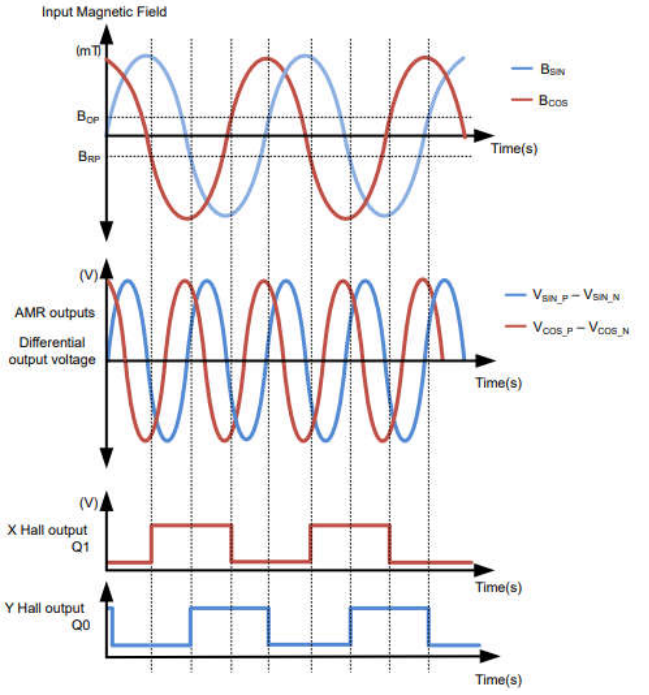

Figure 5. *TMAG6180-Q1 output waveforms.*

For better accuracy, the MCU should integrate a high-speed, high-ENOB analog-to-digital converter, be able to run a digital filter such as a finite impulse response filter to eliminate signal-chain noise, and have an additional compensation algorithm to eliminate errors caused by mechanical tolerances and the signal chain's gain and offset mismatch. The **High-Resolution, Low-Latency, Compact Absolute Angle Encoder Reference Design with AMR Sensor** is a small-form-factor (3cm diameter) reference design with the TMAG6180-Q1 and **MSPM0G3507** MCU, with integrated dual 12-bit ADCs up to 128X oversampling and a math accelerator to help improve efficiency and reduce system cost. The system achieves an angle measurement with a 94.7dB SNR equivalent to 15.4 ENOB and an angle error below 0.05°, as shown in **Figure 6**.

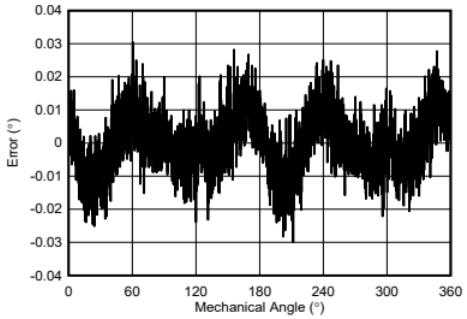

Figure 6. *Angle error over one revolution with offset calibration at 25°C.*

Inductive position sensing

Inductive angle sensors offer some advantages over magnetic sensors. Their main advantage is inherent magnetic immunity to external DC fields. Additionally, inductive technology requires only a conductive metal target – and no magnet – to be in proximity with the sense coils in order to determine the metal target position as it spins about the shaft.

Figure 7 shows an absolute encoder using two **LDC5072-Q1** inductive sensors, one for each sense coil. Nonius encoding requires two sense coils: the outer sensor target may have 16 metal positions; the inner target, 15. Evenly spacing both targets forces a unique

pattern across a complete rotation, providing the ability to know the absolute angle with high precision.

Mechanical resolvers perform the same function as absolute inductive encoders, but have size and weight disadvantages. It is possible to build inductive encoding solutions directly on a printed circuit board, while resolvers are built on thick steel laminations with copper-wire-wound teeth. Resolvers are also expensive to build because of their mechanical structure. Finally, power consumption can be an issue, as resolvers easily consume 500mW of power (assuming 70mA at $7V_{RMS}$).

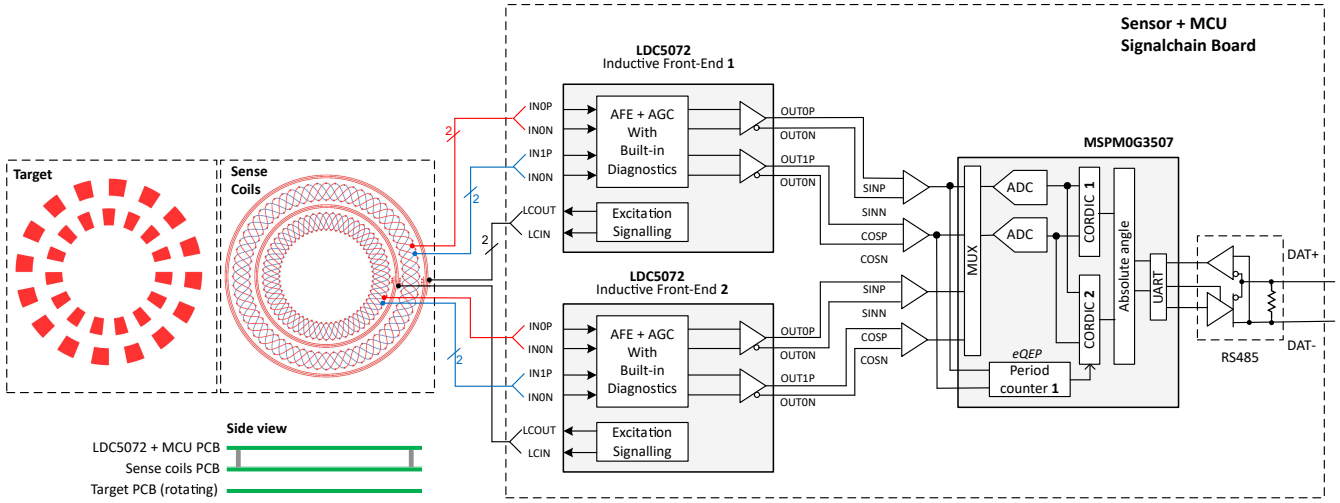

Figure 7. *Absolute encoder with the LDC5072-Q1.*

Conclusion

Selecting the most appropriate position sensor depends on motor-drive system requirements, with cost, performance, operating temperature and size the most important trade-offs to consider. Another aspect is whether to add additional diagnostics or functional safety to an industrial or automotive solution. Each motor and encoder type have their own requirements, so it's important to choose the best sensor type for the application.

Additional resources

- Read the application brief, **Motor Control in Humanoid Robots**.
- Check out the **Absolute Angle Encoder Reference Design with Hall-Effect Sensors for Precise Motor Position Control**.

A novel approach to narrowband matching high-speed RF ADCs

Rob Reeder
Application Engineer
High-speed data converters

For applications that don't require wideband sampling (1GHz to 2GHz or more), it can be challenging to design a narrowband (NB) match (requiring only hundreds of megahertz) with a balun or transformer front-end circuitry for an analog-to-digital converter (ADC). This challenge is magnified in systems with high intermediate frequencies that are digitized in modern communications or radar systems to perform signal processing in the digital domain.

In this article, I'll describe a simple process to maximize your ADC without a lot of simulation downtime. In a few simple steps, this process resolves hundreds of megahertz of bandwidth (BW) at any baseband or intermediate frequency location, as long as it sits within the ADC's own rated bandwidth.

Choosing the ADC and balun

Understanding the application requirements upfront is crucial when selecting the right type of ADC and ultimately determining the front-end development approach. Assume that there is a defined sampling rate, number of channels, digital output interface type and useful internal digital features that you could use or that are necessary for the application. I'll use the ADC3669 converter throughout this narrowband front-end example.

To begin, you must first understand the analog input characteristics of your chosen ADC. If you scroll down to the analog input parameters section of any converter datasheet, you should see the parallel R||C specified in the specification tables. If not, check whether there is a simplified analog input model. As a final option, use the ADC's S-parameters, which are typically listed on the product's webpage. For example, the ADC3669 data sheet lists a model input with a resistor (R) = 100Ω and a capacitor (C) = approximately 1.85pF (aggregated) differential impedance terms. See Figure 1.

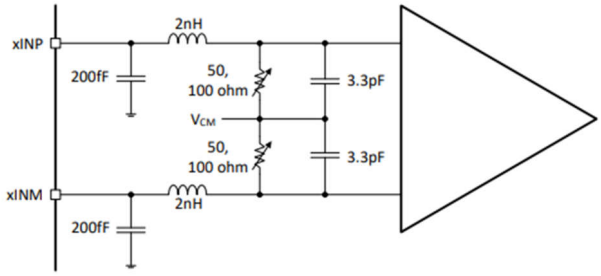

Figure 1. *Analog input model in the ADC3669 datasheet*

The next step is to choose the proper transformer or balun for the ADC, which include comparing these specifications between vendors: the return loss (RL), insertion loss, and phase and magnitude imbalance. If these parameters are not specified on the data sheet, ask the manufacturer, or measure them using a vector network analyzer or VNA.

Choosing between a standard flux-coupled transformer or balun will depend on the BW requirements. Standard transformers are often <1GHz, whereas a balun can achieve much higher BW. Reference [1] describes transformer and balun parametric and ADC requirements in detail.

For NB matching, the example calls for a reactive resistor-capacitor-inductor (RCL) match with the last component in shunt; see Figure 2 and References [2] and [3] for information about matching pads and topologies. Collecting and understanding the application

requirements will enable you to select the front-end BW and balun. For the example, I selected the TCM2-33WX+ balun from Mini-Circuits with a 1:2 impedance ratio and 3GHz of BW after measuring and understanding this balun's capabilities from previous examples used on the ADC3669 evaluation module (EVM). The TCM2-33WX+ provides a relatively low input drive in order to reach ADC's full scale input range.

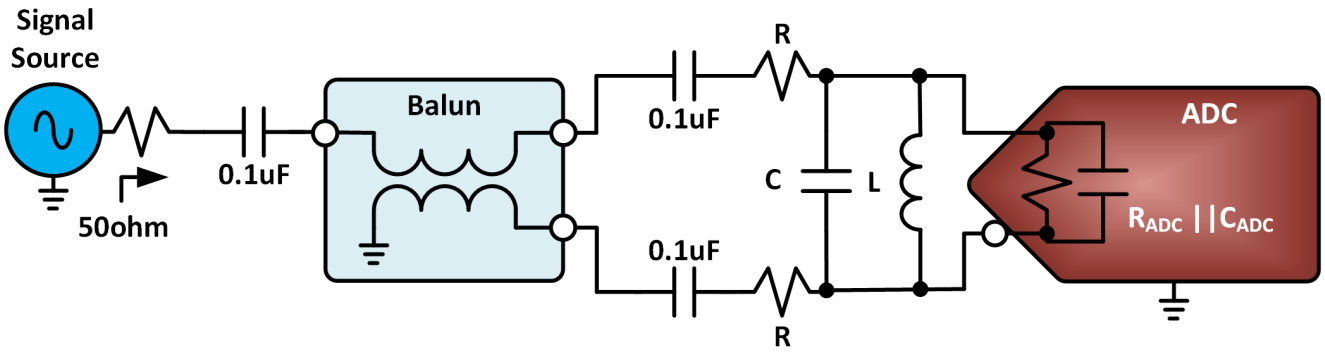

Figure 2. *Front-end interface and component placement*

Solving for R

To conduct an RCL reactive match, first determine the R value of the front end. You could split the termination between the primary and secondary of the balun, but in this example we only terminate the secondary of the balun in order to minimize the number of components required. Depending on the application and signal-chain lineup, a split termination across the balun's primary and secondary may make more sense.

As shown below, the calculations reveal how to solve the R value which completes the differential termination required by the secondary of the balun. A good starting point for setting up the secondary differential termination is to use the ideal case, 100Ω, since this balun has an 1:2 impedance ratio. The balun does have losses and parasitics that change over frequency. So, to start the calculation and obtain a more proper R value termination, use the balun's RL number at the specified center frequency (940MHz in the example) to calculate the characteristic impedance (Zo) to which the balun needs to be properly matched for optimized signal power transfer to the load.

The example illustrates how to calculate the secondary termination of the balun chosen. The TCM2-33WX+ data sheet specifies –16.3dB at 940MHz. Using this value, solve for the characteristic impedance as reflected from the balun's secondary (Equation 1):

$$RL = -16.3dB \text{ at } 940MHz = 20\log\left(\frac{50-Zo}{50+Zo}\right) = 10^{\left(\frac{-16.3}{20}\right)} = \left(\frac{50-Zo}{50+Zo}\right) \quad (1)$$

Therefore, Zo = 36.72Ω (primary impedance).

In an ideal 1:2 impedance balun, 100Ω on the secondary should equal 50Ω on the primary; see Figure 3. This is not the case in actuality, however, as shown in the calculation. To determine the actual impedance reflected back to the primary, use the value of Zo found in the previous step, and back-calculate to get the proper termination on the secondary side (Equation 2):

$$\frac{Z(Primary\ Reflected)}{Z(Secondary\ Ideal)} = \frac{Z(Primary\ Ideal)}{Z(Secondary\ Reflected)} \quad (2)$$

Therefore, $\left(\frac{36.72}{100}\right) = \left(\frac{50}{X}\right)$, where solving for X = 136.1Ω.

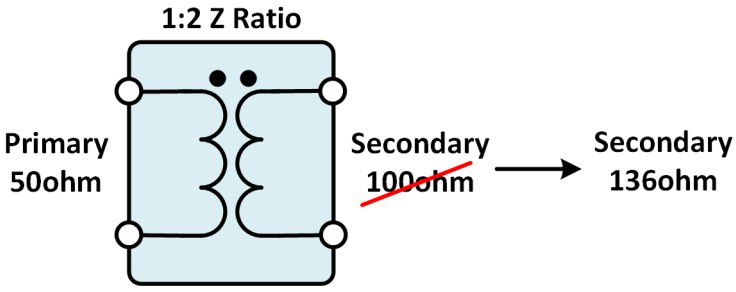

Figure 3. *A 1:2 impedance balun or transformer*

Because the balun has some unaccounted losses at this frequency, the 136Ω secondary termination helps compensate for these losses and provides a better termination value to start with on the secondary, reflecting back the correct impedance at this specific intermediate center frequency onto the primary of the balun. Proper impedance matching will achieve a closer 50Ω match on the primary to yield the maximum signal power transferred from the source.

The 136Ω secondary termination is an aggregate termination. Because the ADC itself already has a 100Ω differential termination inside, place one series 33Ω resistor on each side of the secondary. Review Figure 2 again. You have now solved for the R value required.

A –16dB RL at 940MHz may allow you to use smaller resistor values or possibly eliminate them altogether. I recommend keeping resistors in the design, however, as the ADC's internal differential impedance has a ±10% tolerance range from process variations; the RL of the balun will have tolerances as well. Adding in a small amount of extra resistance helps keep the overall impedance more accurate, as you will notice when looking closely at the ADC's S-parameter values at 940MHz.

Solving for L

The next step is to "resonate out" the ADC's internal C to determine an equivalent shunt inductor or L value for the match. To choose this value, first find the internal C value of the ADC using one of two methods:

- Use the ADC model given in the data sheet (Figure 1) to determine the aggregate parasitic internal front-end capacitance or C value, estimated as approximately 1.85pF.
- Use the S-parameters from the ADC3669 webpage. See reference [4].

The second approach offers a more precise capacitive number at the frequency of interest, as the capacitive value found at 940MHz will be more absolute versus the first approach, where the C value in the model covers the full range of the ADC's input BW. Let's review both approaches in order to understand the trade-offs.

In both methods, the idea is to simply set the two reactive elements to be equal (Equation 3):

$$X_C = \frac{1}{(2\pi \times f \times C)} \; and \; X_L = 2\pi \times f \times L \tag{3}$$

Next, set f to the resonate center frequency of your NB application. For the example, I will use 940MHz.

In the first method, if f = 940MHz,

$$\frac{1}{(2\pi \times 940M \times 1.85p)} = 2\pi \times 940M \times L \tag{4}$$

Then, solving for L = 15.5nH.

In the second method, you need to use the S-parameters and plot them in a simulator in order to determine the C value at 940MHz; see Figure 4.

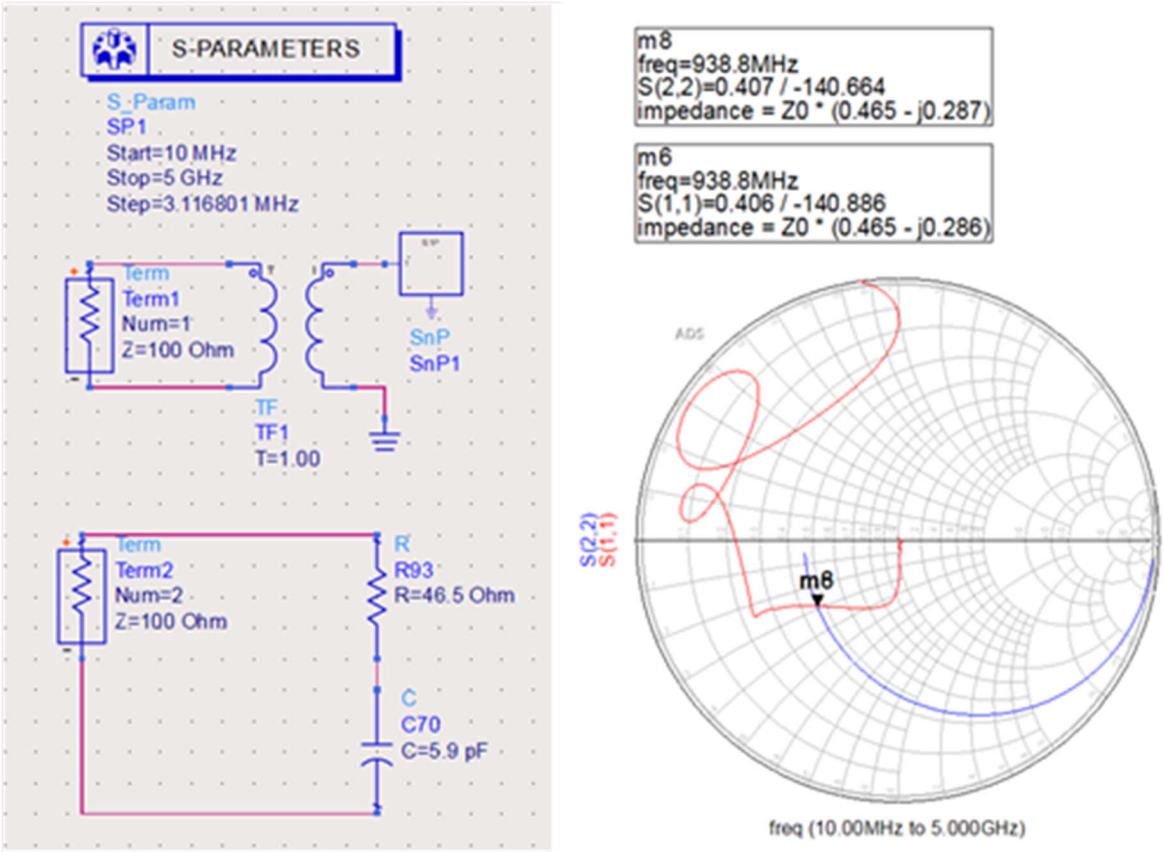

Figure 4. *Smith chart plot of the ADC3669 analog input at 940MHz*

The second method is a bit more involved; the Smith chart plots the S-parameters in a series R + jXc configuration. The R + jXc needs to be parallel-transformed so that the R and Xc are in parallel, or R||Xc. See Figure 5 and Equation 4:

$$Impedance = Z_o \times (R + jX_c) \; or \; 100 \times (0.465 - j0.287) = 46.5 - j28.7 \quad (5)$$

Use Equation 5 to obtain the parallel transformation:

$$R_p = \left(\frac{46.5^2 + -28.7^2}{46.5}\right) = 64.2\Omega \quad (6)$$

Recalling the two inflated 33Ω resistors used to set the R value in the previous section brings the aggregate resistive termination seen by the balun to 130.2Ω, which is closer to 100Ω differential that the balun would see ideally with a smaller or no R value at all.

Next, solve for the parallel capacitor at 940MHz, see Equation 6:

$$C_p = \frac{\frac{-28.7}{(46.5^2 + -28.7^2)}}{\frac{2}{\pi \left(-28.7 \times 10^6\right)}} = 1.62pF \quad (7)$$

Now use the same equation as above in order to find the appropriate shunt L value. If f = 940MHz, C = 1.62pF, then $\frac{1}{(2\pi \times 940M \times 1.62p)} = 2\pi \times 940M \times L$. Solving for L = 18.1nH.

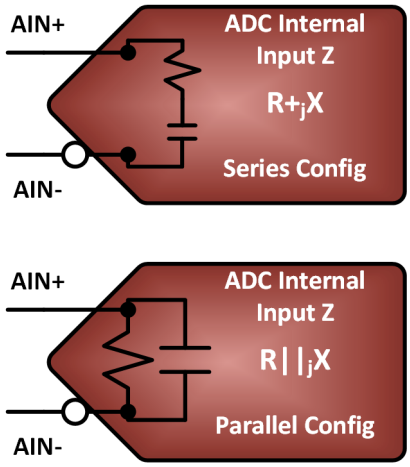

Figure 5. *ADC internal R and C series to parallel representations*

These two C values found in the two methods above (eg: 1.85pF and 1.62pF) are on the order of the same magnitude; therefore, you need to consider the internal inductive L parasitics, as well as the external L parasitics that get added in, based on your layout.

It is also possible to simulate the entire frontend in ADS simulator package, as shown in Figure 6, which uses the S-parameters of the TCM2-33WX+ balun and the ADC3669. The simulation results shown in Figure 7 show very good RL (<–15dB), indicating that 18nH is a good match at 940MHz.

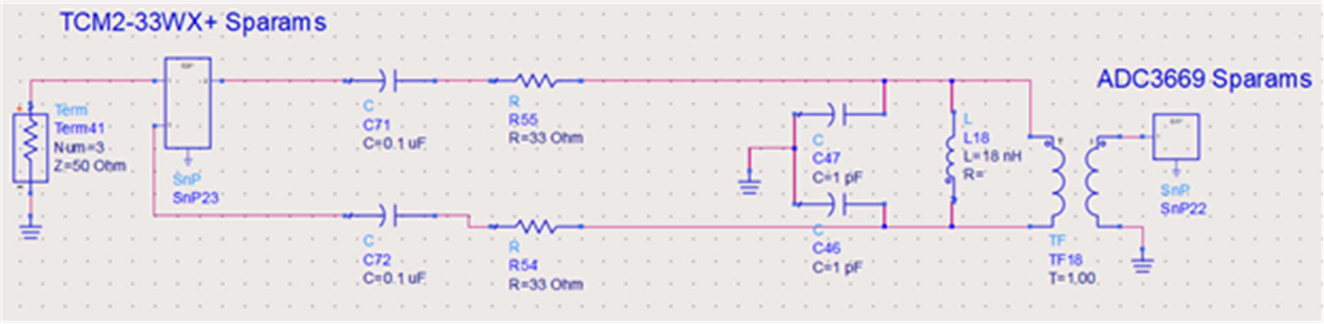

Figure 6. *ADS simulation front-end mockup with 18nH shunt match*

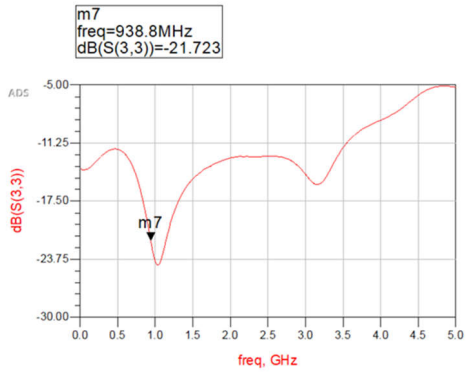

Figure 7. *Simulated RL (S11) plot of 18nH shunt-matched response*

Next, let's compare our simulated results against some measured data in the lab. Figure 8 illustrates the use of the ADC3669 EVM to implement the front-end match to measure a passband flatness response. The resonant point is centered, but the match is a bit more wideband than expected. This is where simulation can be inadequate. A 3D electromagnetic simulation solver might be able to capture all of the board parasitics in order to get a closer 1:1 match between the simulation and lab measurements. There are a few second- and third-order nuances to uncover, however. Next, we will add in a shunt C to complete the RCL reactive match to make the lab measurement narrower, as expected.

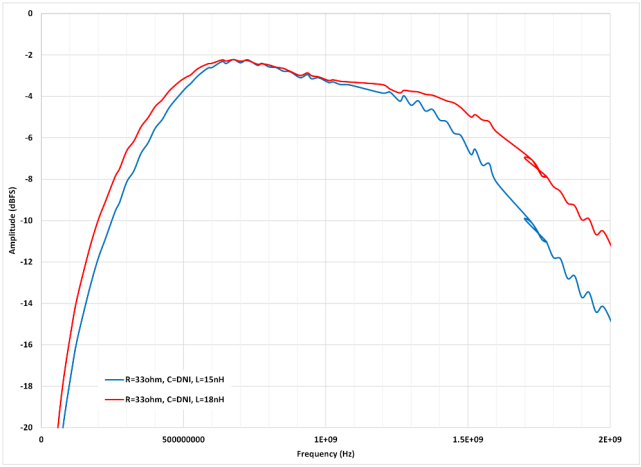

Figure 8. *Passband flatness sweep with L value installed*

Solving for C

To further improve the narrowband width match (in other words, make it narrower), add the last component in the RCL reactive match from Figure 2. Placing the C term in parallel with the inductor creating an LC tank. It seems counterintuitive to add capacitance back into the front-end match after placing the 18nH inductor to combat the ADC's internal capacitance, but it tightens the filter match. In order to solve for a parallel C value to complete the LC tank, use Equation 7:

$$f_o = \frac{1}{(2\pi \times \sqrt{LC})} \; or \; 940MHz = \frac{1}{(2\pi \times \sqrt{18n \times C})} \quad (8)$$

Solving for C = 1.6pF.

Let's put this value (1.6pF capacitor or nearest standard value) in the front-end design and rerun the passband BW sweep; see Figure 9.

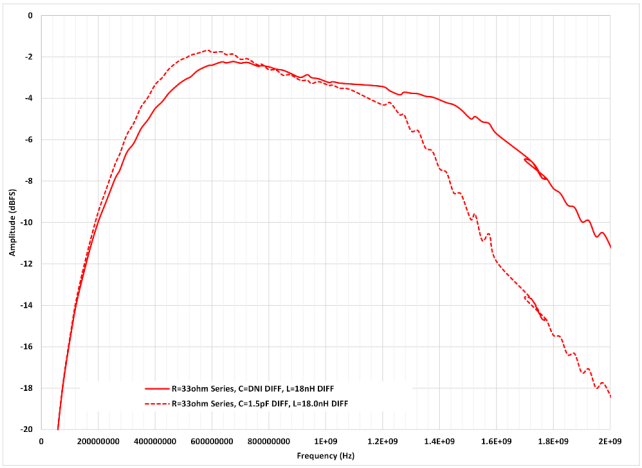

Figure 9. *Passband flatness sweep with L and C values installed*

As can be seen, adding in the additional 1.5pF capacitor in parallel with the 18nH inductor, creating that LC tank, doesn't really improve or narrow the match (see mini-dashed curve).

The LC tank method will work, but with a few considerations. Removing the internal C by solving the external L value (18nH) will help but may not entirely prove to be the end solution. To implement this accurately, you need to use a much larger C value to completely remove any internal and residual external C parasitics. You are competing with balun and trace parasitics, as well as the ADC's internal sampling capacitor, which is dynamic in nature as the sample switch opens and closes quickly.

Let's choose a higher value for C, such as 9.1pF, re-solve for L in using Equation 7 again:

$$f_o = \frac{1}{(2\pi \times \sqrt{LC})} \; or \; 940MHz = \frac{1}{(2\pi \times \sqrt{L \times 9.1p})} \quad (9)$$

Solving for L = 3nH.

With these values in place of the front-end design, Figure 10 shows the results after re-running the passband BW sweep.

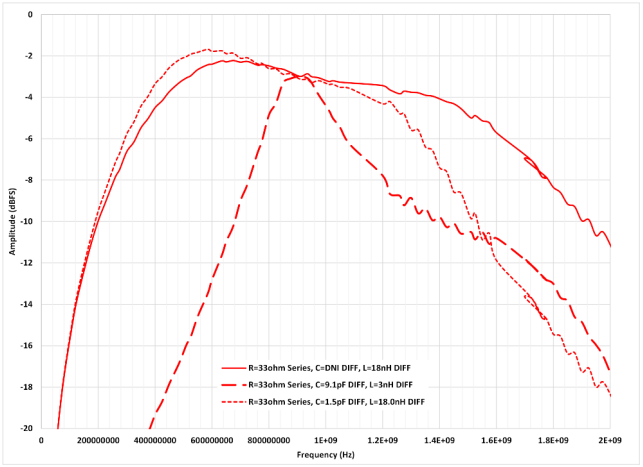

Figure 10. *Passband flatness sweep with new L and C values installed*

As you can see, there is a considerable improvement when narrowing the bandwidth match to 350MHz wide (the thick dashed curve) by increasing the external C in order to further improve the NB match response. Typically, it's good to use at least twice the value of C based on the aggregate ADC's internal sampling network as a good starting point. Adding this term externally will only further improve RL in the band of choice.

You can then adjust the L value, the C value, or both to help widen or narrow or shift the BW needed to match

for your application needs. You will need to remember these values for the layout, balun and ADC input model; it is not possible to simulate all parasitic nuances, and some empirical experience might be necessary in order to gauge the match properly.

Figure 11 illustrates the signal-to-noise ratio (SNR) and second- and third-order harmonics (HD2 and HD3) collected over the NB application example to further verify the ADC's performance within the 940MHz band.

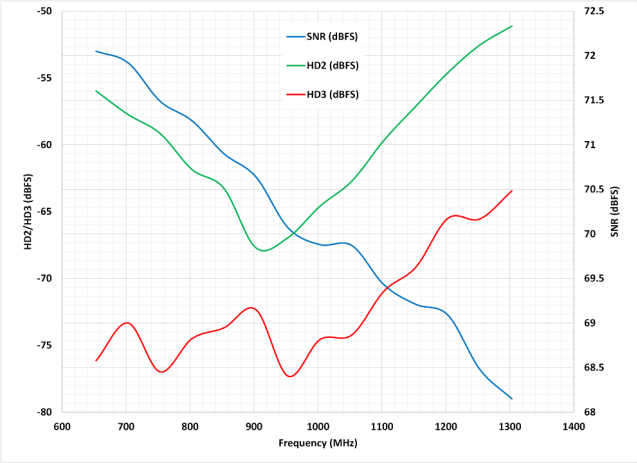

Figure 11. *Resulting AC performance of SNR, HD2 and HD3 vs. the NB match frequency range*

An analog input center frequency of 940MHz is a bit outside the ADC datasheet measurement specification. The collected values do follow the correct trend for all the collected measurements, SNR, HD2 and HD3, however, and degradation will continue to occur as the input RL degrades >940MHz for this particular ADC.

Conclusion

You do not have to be an expert simulator when developing a narrowband matching application to your particular high-speed RF sampling ADC. This NB matching approach can be used to help strengthen any upstream filtering in the RF signal chain. First, address the resistive part of the NB matching effort by using the chosen balun's return loss values from its datasheet to will help improve the input front-end network's return loss. Next, use the ADC's given S-parameters, datasheet input model or lumped element R||C values in the specification tables as a starting point to your NB match, at your frequency band of interest. Keep in mind, the balun and pcb layout contribute to the passive components needed to complete the match. Make sure these are factored in as well as a starting point.

With a little simulation to provide direction and some simple math, you can accelerate your next high-speed RF converter design in no time.

References

1. Reeder, Rob. "**Comparing Active vs. Passive High-Speed/RF A/D Converter Front Ends**." Texas Instruments application note, literature No. SLAAET1, March 2025.
2. Reeder, Rob. "**The 3rd dB: Why a Lossy Attenuation Network Pad Works Well With RF ADCs**." Texas Instruments application note, literature No. SLVAG01, February 2025.
3. Reeder, Rob, and Luke Allen. "**The Fine Art of Passive Matching a High-Speed A/D Converter Analog Input Frontend**." Texas Instruments application note, literature No. SBAA665, December 2024.
4. Texas Instruments. n.d. **ADC3669 evaluation module**. Accessed Sept. 23, 2025.
5. "**ADC3668, ADC3669 Dual-Channel, 16-Bit 250MSPS and 500MSPS Analog-to-Digital Converter**." Texas Instruments data sheet, literature No. SBASAL3B, September 2024, revised June 2025.
6. "**TCM2-33WX+ Surface-Mount RF Transformer**." Mini-Circuits data sheet, literature No. ECO-013812.
7. Keysight Technologies. n.d. **Advanced Design System (ADS) market-leading circuit design and simulation software**. Accessed Sept. 23, 2025

Cascaded ideal diodes: Solving 48V EV power challenges

Shiven Dhir
Applications Engineer
Input Power Protection and Distribution

Rakesh Panguloori
Applications Manager
Input Power Protection and Distribution

The increased use of 48V battery subsystems, in addition to conventional 12 V networks, is causing a noticeable change in the design of HEV/EV power systems. 48V delivers more power without the penalty of heavy cabling to reduce the power loss in the wire harness leading to extended drive range. With this change, the vehicle power distribution architecture is transitioning from traditional centralized to zonal approach where power distribution, communication and load actuation are grouped together based on location in the vehicle rather than by function, as shown in **Figure 1.** Zonal architecture reduces system complexity and gives original equipment manufacturers (OEMs) more modularity.

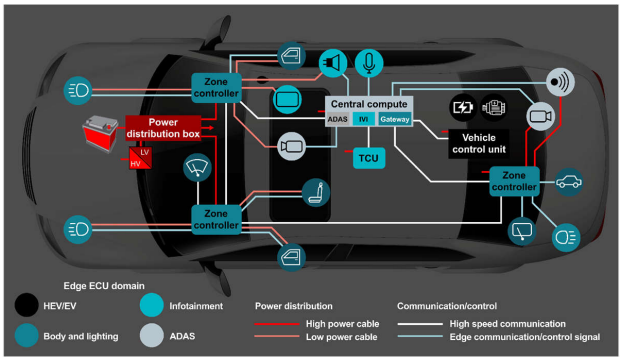

Figure 1. *A zone architecture in a modern vehicle*

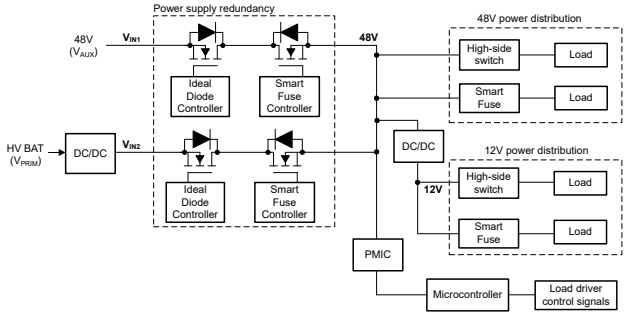

Figure 2. *Typical power distribution in a zone control module*

Figure 2 shows a typical power distribution where multiple power sources are used to realize redundant power supply for a zone control module. Ideal diodes, as discussed in the white paper, "**Basics of Ideal Diodes**," are great for applications that require reverse current blocking and/or reverse polarity. Since ideal diodes offer reverse current protection, they are also useful in applications where combining multiple supplies increases system redundancy **[2]**. However, the existing ideal diode controllers in the market are only rated for 72V absolute max and have limitations to support certain 48V system designs.

This article discusses the challenges of designing an ORing stage for a 48V system and how a cascaded ideal diode configuration enables a reliable ORing solution to safely handle the input supply interruptions and external transient events.

Challenge 1: High voltage stress during reverse supply fault

As seen in **Figure 2,** primary power distribution requires seamless power. High voltage battery (VPRIM) is stepped down by a DC/DC converter for a 48V rail and then a backup 48V auxiliary supply (VAUX) provides a redundant supply when ORed. In case of reverse polarity fault at VIN1, the DC/DC converter output VIN2 powers the entire load as shown in the simplified illustration **Figure 3**. However, this causes high voltage stress for the ORing on the auxiliary supply path. A 48V source can reach a maximum of 54V to create the large voltage difference of 108V between CATHODE to ANODE pins of the controller **LM74700D-Q1**, exceeding the absolute max rating of 75V. The solution also requires at least 120V-rated MOSFETs that are comparatively more expensive than 60V FETs and are hard to multi-source.

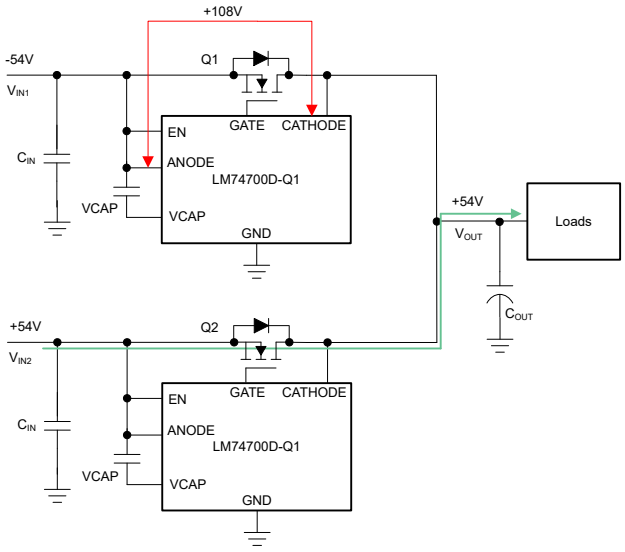

Figure 3. *Voltage stress under input reverse polarity condition*

Challenge 2: Compliance to LV148 load dump and switching transients

Transient overvoltage may occur in the electric system due to the switching off loads and short accelerator tip-ins. For 48V systems, the standards available today (ISO 21780 and Liefervorschriften [LV] 148) specify the E48-02 transient overvoltage profile, shown in **Figure 4**. This profile goes up to 70V and stays there for 40 ms, and some OEMs even require 100ms. The device under test (DUT) must survive these events with Functional Status A, and the DUT must perform all the functions. Note that clamping using TVS or Zener diodes is impractical for such high power and wider transients. Simply said, integrated circuits connected directly to the 48V rail must withstand 70V under all conditions. But. when factoring for switching transients or component margin, the devices should support much greater than 70V. The existing ideal diode controllers with 72V absolute max rating from ANODE to GND leave less margin for the system designers.

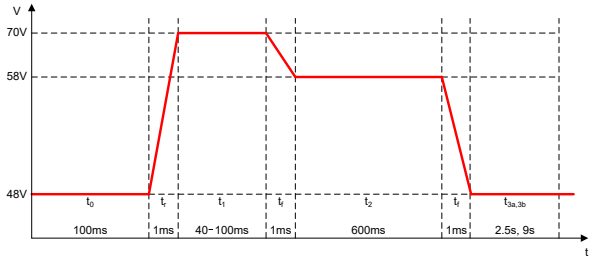

Figure 4. *The E48-02 transient overvoltage profile from LV 148*

Single controller-based solution

Figure 5 shows a solution using a single **LM74700D-Q1**, but using a Zener clamp circuit reduces the large voltage difference of 108V between the CATHODE to ANODE pins of the controller. The Zener diode DZ can limit the voltage between CATHODE to ANODE below its absolute max rating (75V) and the resistor RZ can bias DZ appropriately. However, the solution still requires at least 120V rated MOSFETs which are comparatively expensive than 60V FETs and are hard to multi-source. Also, in normal operation the resistor RZ causes additional drop in the CATHODE path, which impacts the reverse current protection threshold.

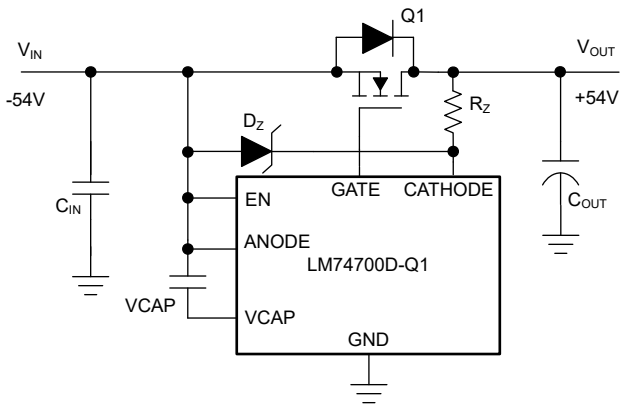

Figure 5. *Solution with single high voltage MOSFET*

Proposed cascaded ideal diode configuration

The proposed solution uses two ideal diode controllers with respective MOSFETs Q1 and Q2 connected in series configuration, as shown in **Figure 6**. The clamping circuits of each controller not only ensure keeping CATHODE to ANODE below 75V but also act as an equalizing network to share equal voltage between Q1 and Q2 during fault events. Let us consider how the circuit works for two common fault scenarios

Case 1: During startup, with the output (VOUT) powered at 54V and input VIN at 0V, the mid-point voltage VMID stays at 0V. The second **LM74700D-Q1** controller keeps GATE2 shut-down due to reverse current blocking scenario with VOUT > VMID and Q2 blocks 54V. In this case, the user applies reverse voltage of 54V at VIN, and the first LM74700D-Q1 controller keeps GATE1 in OFF state due to a reverse polarity scenario with ANODE < 0V and Q1 blocks 54V.

Case 2: In this scenario, VIN starts in fault state (at -54V, for example) and then the system is powered up with VOUT = 54V. The mid-point voltage VMID stays at 0V as the first **LM74700D-Q1** controller keeps GATE1 in OFF state to block reverse voltage at VMID. Similarly, the second **LM74700D-Q1** controller keeps GATE2 shut-down due to reverse current blocking condition. Both MOSFETs Q1 and Q2 incur voltage stress of 54V. Because the voltage across MOSFETs is below 60V during the fault cases, the solution provides flexibility for the customer to select legacy 60V-rated FETs that are easy to multi-source.

As seen in **Figure 6**, the solution also incorporates a transient clamping network (DC, Q3, RB and DB) in the ground path to handle switching transient voltages beyond the absolute max rating of the LM74700D-Q1. In normal operation, the potential difference between device ground and system ground is just VBE of Q3, but whenever VIN exceeds the breakdown voltage (VBR-DC) of diode DC, the transistor Q3 drops voltage across it and lifts up the device ground potential. This helps to limit the ANODE-GND voltage of the **LM74700D-Q1** close to the breakdown voltage of DC, facilitating a scalable transient handling solution. The purpose of diode DB is to block the reverse current path under input supply reverse condition.

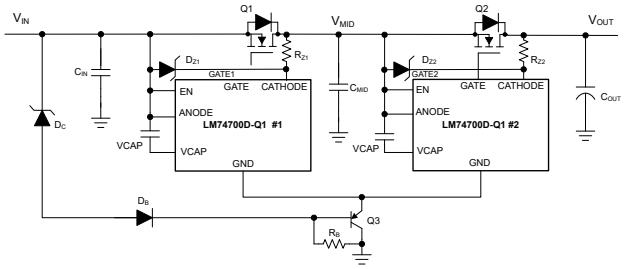

Figure 6. *Cascaded ideal diode configuration*

Component selection and test results

It is important to consider how to select the key components in the system to achieve these results.

For the **Ideal diode MOSFETs Q1 & Q2**, a 60V VDS(MAX) with +/-20V VGS(MAX) provides enough margin for all the fault conditions. RDS_ON at nominal current: (20 mV/ Nominal Current) ≤**RDSON**≤ (50mV/Nominal Current) is important to have lower reverse current. For example, in a 5A design, RDS_ON ranges from 4 mΩ to12.5 mΩ.

The MOSFET gate threshold voltage Vth should be at 2V maximum.

The **PNP transistor Q3** sees the maximum voltage drop after the Zener diode DC is activated and should be rated for voltage greater than (VIN-MAX – VBR-

DC). It also must support the quiescent current of the LM74700D-Q1, which is less than a mA. A transistor like BC857-Q can be used.

For **Zener diodes DZ1 & DZ2:** a 62V Zener like BZX84J-B62 should be chosen to limitCATHODE to ANODE below 75V.For **Zener diode DC,** the breakdown voltage (VBR-DC) of DC determines the clamping voltage between ANODE-GND pins for switching transients on VIN. Utilizing a 62V Zener like BZX84J-B62 can limit the voltages with enough margin for the LM74700D-Q1.The **blocking diode DB** should have blocking voltage capability close to the maximum input supply reverse voltage, so choose at least a 60V-rated diode like the NSR0170P2T5G.

Resistors RZ1 & RZ2are biasing resistors for DZ1 & DZ2. Any value in the range of 1 kΩ to 2 kΩ should be sufficient. **Resistors RB** is the biasing resistor for DC, and any value in the range of 10 kΩ to 47 kΩ will suffices.

Figures 7 and **8** show the drain-source voltage distribution across MOSFETs when input reverse polarity is applied before system startup and after system startup. As seen, the MOSFETs share equal voltage with maximum voltage of <60V across each MOSFET. **Figure 9** shows the performance of the ground path transient clamping network where the ANODE to IC-GND is clamped to 62V for 70V load dump event at VIN.

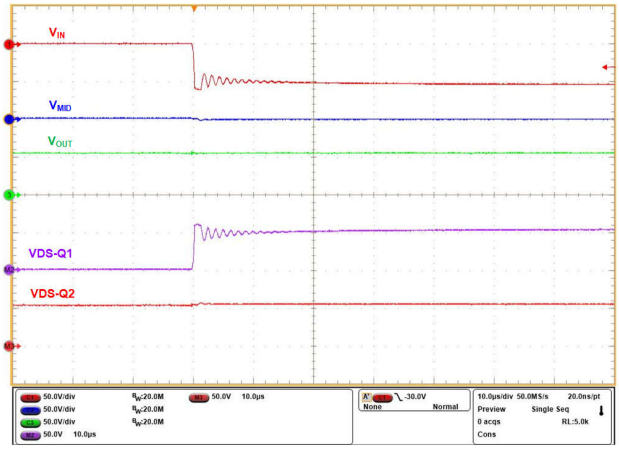

Figure 7. *Voltage sharing across MOSFETs during input reverse polarity condition*

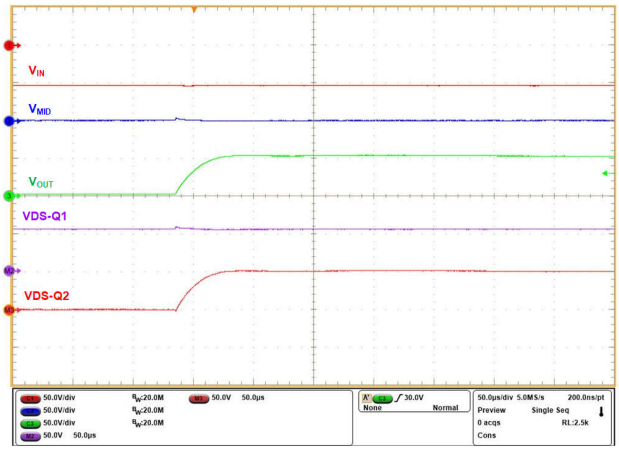

Figure 8. *Voltage sharing across MOSFETs during hot-plug at the output (VIN = -54V)*

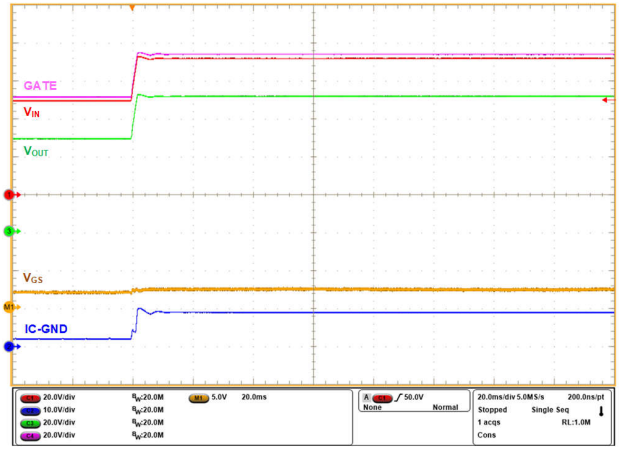

Figure 9. *Response of proposed solution to 70V load dump event*

Conclusion

While 48V systems offer many benefits, they also bring a new set of challenges for redundant supply ORing in power distribution stages. The proposed cascaded ideal diode configuration with ground path transient clamping network enables system design with legacy 60V-rated FETs that are easy to multi-source. The proposed approach also provides adequate voltage margin for switching transients, enabling a reliable ORing solution in 48V systems.

References

1. **Basics of Ideal Diodes**" Texas Instruments application report, literature No. SLVAE57B, February 2021.
2. "**Redundant supply topologies for automotive applications using ideal diode controllers**" Texas Instruments Analog Design Journal, literature No. SLYT848, March 2024.
3. Texas Instruments, **LM74700D-Q1 Automotive Low IQ Reverse Battery Protection Ideal Diode Controller**, Data Sheet.

Comparing discrete and integrated difference amplifiers

Esteban Garcia
Product marketing engineer

Jacob Nogaj
Applications engineer

One of many useful circuits that you can create using an operational amplifier (op amp) and resistor network is a difference amplifier (DA). DAs allow you to measure the difference between two signals, which is useful for current and voltage sensing in systems such as solar panels, power banks and other DC/DC modules. Furthermore, many DAs can apply gain, add a reference voltage to the signal, and reduce common-mode noise from input signals.

There are two main types of DAs: discrete (with external resistors) and integrated (with monolithic or on-die resistors). In this article, we'll use measured data (offset voltage, common-mode rejection ratio [CMRR], gain error and gain error drift over temperature) to compare discrete and integrated DAs.

Gain error

As shown in Figure 1, a typical DA comprises an op amp and four resistors. The midpoint of the R1/R2 resistor ladder connects to the inverting terminal of the op amp, while the R3/R4 midpoint connects to the noninverting terminal.

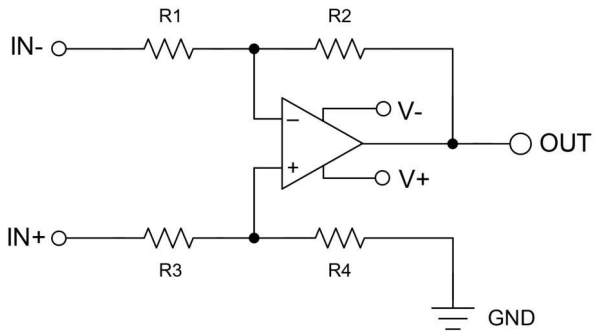

Figure 1. *A typical DA*

Equation 1 depicts the transfer function of a typical DA. Notice that the ratio of R2 and R1 (assuming that R1 = R3 and R2 = R4) determines the gain. You will need matched resistors if you are trying to achieve a low gain error. Resistors with a tolerance of ±1% can induce a gain error as high as 2%. While discrete resistors may exhibit large variations, the monolithic resistors found in integrated DAs are often trimmed to achieve a gain error of just 0.01%.

$$V_{OUT} = (V_{IN+} - V_{IN-}) \times \left(\frac{R2}{R1}\right) + V_{REF} \quad (1)$$

Gain error drift

Gain drift is another important parameter, especially in systems such as solar panels, motor drives and battery packs where temperature can fluctuate throughout the day or throughout operation. Because the thin-film resistors of TI's **INA600** DA are all within the same package and interdigitated with each other, all four resistors will equally observe any temperature fluctuation, making them drift together while maintaining the same gain ratio. A discrete implementation using external resistors may observe wide variances in the gain drift performance of your DA, since the stress from the temperature will appear as a gradient across the surface of the board, leading to changes in the applied gain to your input signal.

Offset voltage

When applying gain to an input signal, the amount of offset voltage can significantly influence the amount of error induced on the output signal. Therefore, we recommend selecting an op amp with an excellent offset voltage for any voltage or current sensing. When building a discrete DA, you have the flexibility to use whichever available op amp is at the core of your design, whereas the offset voltage of an integrated DA will be fixed and dependent on the internal op amp. With resistor trimming techniques such as the e-Trim™ operational amplifier technology, it is possible to lower the offset voltage in an integrated DA, however.

CMRR

The ability to reject common-mode signals in voltage- and current-sensing applications is a primary factor when considering a DA. Similar to gain error, the CMRR will depend on the matching of the components (such as resistors) used. While a typical op amp may have a CMRR as high as 100dB, introducing mismatched resistors could drop the CMRR as low as 60dB, making them nonideal for industrial systems in noisy environments. The CMRR of a typical integrated DA will generally be at least 90dB, but can be as high as 130dB.

Gain configurations enabling beyond-the-rail voltage monitoring

DAs are typically in a unity gain configuration (meaning that the gain = 1) but can vary from 0.5 up to 2. Changing the values of the resistor networks in a DA makes it possible to achieve a wide range of gain ratios for different applications that may require greater attenuation to scale the voltage down to the input range of an ADC (3.3V or 5V). As shown in Figure 2, changing resistor network values achieves greater attenuation.

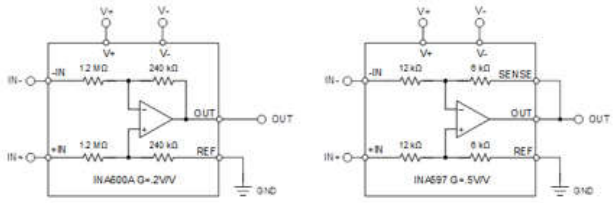

Figure 2. *The INA600A DA vs. the INA597 DA*

An overlooked benefit of DAs is their ability to allow your input to go beyond the rails. Because the resistor ladders divide down the input voltages of the DA, the input of the integrated amplifier will only see the attenuated voltage. With standard op amps, the supply voltage limits the common-mode voltage range. This flexibility of the DA makes them suitable for monitoring higher voltages when the amount of available power rails is limited. As shown in Figure 3, the input voltage range extends further than the recommended supply voltage of the DA.

6.3 Recommended Operating Conditions

over operating free-air temperature range (unless otherwise noted)

		MIN	MAX	UNIT
Supply voltage $V_S = (V+) - (V-)$	Single-supply	2.7	40	V
	Dual-supply	±1.35	±20	
Input voltage range	Single-supply / Dual-supply	(V–) – 40	(V–) + 85	V
C_{BYP}	Bypass capacitor on the power supply pins (1)	0.1		µF
Specified temperature	Specified temperature	–40	125	°C

Figure 3. *Recommended operating conditions of the INA600 DA*

In higher-power-density systems, the increase in switching frequencies and parasitic inductances caused by printed circuit board traces can lead to additional voltage disturbances that affect voltage monitoring accuracy, as common-mode noise cannot be completely eliminated. While using an integrated DA with high CMRR will remove any common-noise observed across the inputs, achieving high CMRR with the external resistors in a discrete DA will be difficult to achieve given the small mismatches of the resistors, especially at higher gain ratios.

Equation 2 expresses how parasitic inductances and switching frequencies influence the amount of voltage disturbance of your signal:

$$V = L \times \frac{di}{dt} \quad (2)$$

Figure 4 illustrates the CMRR performance over frequency for an integrated DA.

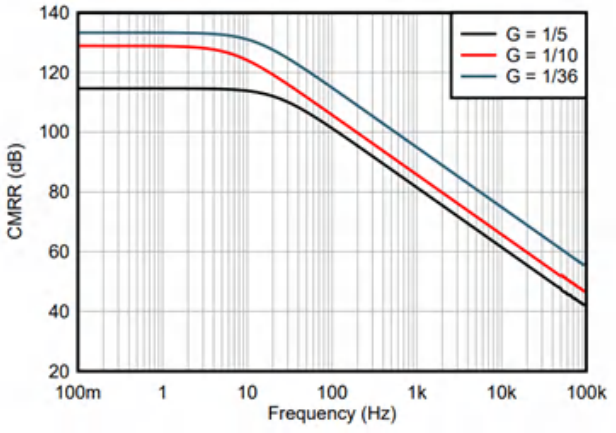

Figure 4. *Output-referred CMRR vs. frequency for the INA600 DA*

Test setup and comparison

We used CMRR and offset voltage errors as a measure of the relative performance of each circuit across temperature. For each device, we connected a precision source measure unit to both input pins of the DA and used a calibrated 8.5-digit multimeter to measure the change in offset voltage. We repeated all testing over five averaged sweeps to obtain an accurate representation of device performance, configuring the devices to sweep a common-mode voltage of -35V to 35V, with a split supply configuration of ±18V. We performed overtemperature testing with an oven, along with sufficient soak time to ensure uniform temperature across the test board.

Forcing a differential voltage across the device inputs while maintaining a common-mode voltage at mid-supply tests both the gain error and gain error drift. Sweeping each device with a corresponding input range forces the output to range from –10V to +10V, enabling you to compare the corresponding slope to the ideal slope and thus evaluate the percentage of gain error.

Table 1 compares the performance of CMRR and the offset between a discrete DA and two TI integrated DAs across different operating temperatures.

	Discrete DA		INA600		INA597	
Temperature (°C)	CMRR (dB)	Offset (µV)	CMRR (dB)	Offset (µV)	CMRR (dB)	Offset (µV)
125	73.06	–237.88	98.33	801.82	102.66	–26.12
85	71.89	–285.95	100.12	661.56	103.70	–10.22
25	70.35	–221.42	101.63	582.19	100.33	–3.24
–40	73.26	–206.95	106.82	500.60	105.97	13.4

Table 1. *CMRR and offset voltage comparison*

Table 2 compares the gain error and drift performance between the same discrete DA and integrated DAs across different operating temperatures.

	Discrete DA		INA600		INA597	
Temperature (°C)	Gain error (%)	Gain error drift	Gain error (%)	Gain error drift	Gain error (%)	Gain error drift
125	0.14806	–237.88	98.33	801.82	102.66	–26.12
85	71.89	–285.95	100.12	661.56	103.70	–10.22
25	70.35	–221.42	101.63	582.19	100.33	–3.24
–40	73.26	–206.95	106.82	500.60	105.97	13.4

Table 2. *Gain error and drift comparison*

As expected, the integrated DAs performed exceptionally well in achieving high CMRR, low gain error and low gain error drift compared to the discrete DA. While the offset voltage of the discrete DA outperformed one of the integrated DAs, it is possible to compensate for this through software calibration.

Figure 5 shows a simplified layout of each of the three DA variants and compares the sizes of each solution. For comparison purposes, we used the smallest device packages, along with resistors and capacitors in the 0402 package.

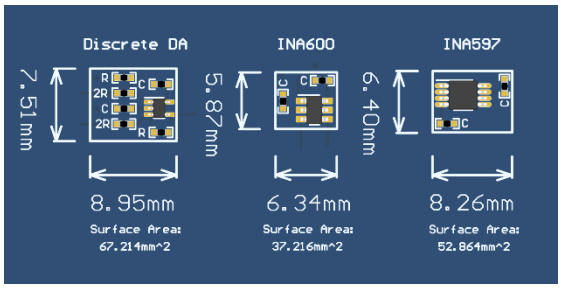

Figure 5. *Size comparison*

Conclusion

While there are many ways to accomplish voltage sensing, an integrated DA provides exceptional performance benefits that are not achievable with a discrete implementation. Input voltage limitations from the supply voltage of op amps become a nonfactor for integrated DAs such as TI's **INA600**, and high attenuation ratios provide flexibility when monitoring voltages beyond the supply rail.

Designing real-time diagnostic circuits for automotive audio applications

Jared Becker
Technical Sales Engineer

Designers of modern in-car audio systems are rapidly adopting diagnostic capabilities to monitor Class-D amplifier integrated circuits and attached speakers. Of key concern are the in-vehicle speakers connected to the telematics control unit (TCU) used during roadside emergency situations, such as a crash or breakdown (Figure 1). Detecting and notifying drivers to shorted or disconnected speakers enables them to schedule maintenance before a catastrophic event.

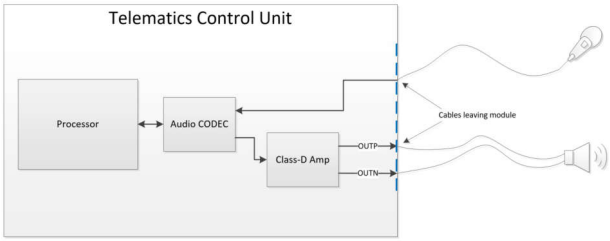

Figure 1. *TCU with a Class-D audio amplifier showing the speaker connection*

Real Time Diagnostics (RTD)

As an additional layer of safety, some vehicle manufacturers are requiring real-time diagnostics (RTD). Traditionally, Class-D speaker diagnostics check the speaker when the TCU module or Class-D amplifier turns on but will not monitor thereafter for all fault scenarios. RTD monitors the speaker at startup and continues to monitor it while the vehicle is in operation. This additional monitoring not only reduces the time between system failure and notification but also ensures prompt notification during events such as a lengthy hundred-mile drive.

Immediately alerting the driver minimizes the chance of an accident occurring while the emergency call speaker is in a faulty condition. Additionally, the system can also alert emergency service operators during an emergency phone call if a speaker fault issue is detected. If the speaker experiences a fault after a car accident (such as severed wires between the TCU module and the speaker), the system can send a message to the emergency operator that the driver will not be able to hear their commands. As a final requirement, diagnostics should never introduce errant audio in the cabin.

The Class-D amplifier must be able to diagnose four main speaker fault conditions, as shown in the following figures.

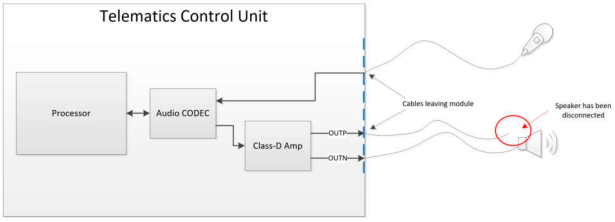

Figure 2. *The four speaker fault conditions: open speaker or load (a); positive output shorted to a negative output (b); positive output or negative output shorted to ground (c); positive output or negative output shorted to the vehicle battery (d).*

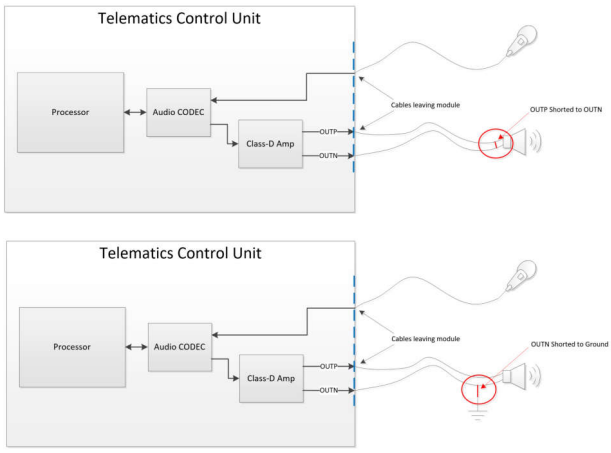

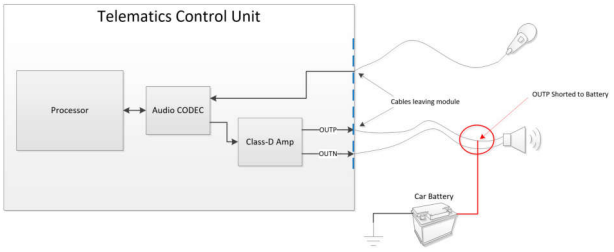

Additionally, the Class-D amplifier should be able to operate normally even when a fault is removed without requiring host intervention. For example, it should be possible to detect an intermittent short on the speaker wires; however, the system still operates normally when the fault condition is removed.

Class-D amplifier selection

The Texas Instruments **TAS5431-Q1** Class-D amplifier can deliver up to 8 W of power to a car speaker and protect itself and the TCU module from four fault conditions, as well as diagnose all four fault types at startup (also known as “deassertion of standby mode”). After startup, the amplifier can detect a positive or negative output shorted to ground, a positive or negative output shorted to the vehicle battery, and a positive output shorted to a negative output only while audio is playing. More details on how the TAS5431-Q1 diagnoses these fault conditions can be found in section **7.3.5 “Load Diagnostics” of the TAS5431-Q1 datasheet**.

Although the **TAS5431-Q1** is capable of diagnosing these fault conditions at startup, it cannot implement the full RTD suite on its own. A notable shortcoming is the inability to detect a positive output shorted to a negative output or an open speaker/load after deassertion of standby mode. Table 1 summarizes the standard capabilities of **TAS5431-Q1** diagnostics.

	Deassertion of standby mode	Device in operation (no audio)	Device in operation (audio playing)
Positive or negative output shorted to ground	Yes	Yes	Yes
Positive or negative output shorted to battery	Yes	Yes	Yes
Positive output shorted to negative output	Yes	No	Yes
Open load	Yes	No	No

Table 1. *TAS5431-Q1 RTD summary*

Achieving RTD

To detect a positive output short to a negative output when no audio is present, the audio source (codec or processor) must mix in a baseline signal with the voice or audio signal (**Figure 3**). As an example, a baseline 5Hz 200mV peak-to-peak signal is well below the audio frequency range (20Hz to 20kHz) and has enough amplitude (200mV peak to peak) to produce the required excitation to detect a positive output short to a negative output.

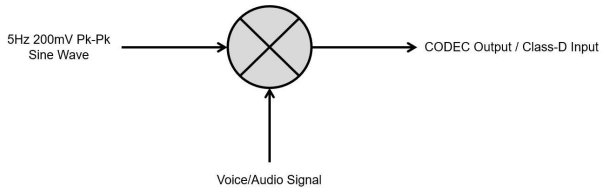

Figure 3. *Mixing in an out-of-band baseline signal of 5Hz at 200mV peak to peak enables detection of output shorts when no audio is present*

Applying a low-frequency baseline signal to the input of the **TAS5431-Q1** ensures that the device will hit its overcurrent limit when a positive output shorts to a negative output. The diagnostic assessment mode integrated into the **TAS5431-Q1** will then detect the positive and negative voltages and report the fault in the register map. Simply implementing this waveform changes the summary of diagnostics, as shown in Table 2.

	Deassertion of standby mode	Device in operation (no audio)	Device in operation (audio playing)
Positive or negative output shorted to ground	Yes	Yes	Yes
Positive or negative output shorted to battery	Yes	Yes	Yes
Positive output to a negative output	Yes	Yes	Yes
Open load	Yes	No	No

Table 2. *Summary of TAS5431-Q1 RTD when adding a baseline 5Hz 200mV peak-to-peak sine wave to the Class-D amplifier input*

Implementing a current-sense resistor, a current-sense amplifier, and a resistor-capacitor (RC) filter (**Figure 4**) in conjunction with the same 5Hz, 200mV peak-to-peak baseline signal enables the system to detect a speaker or open-load condition.

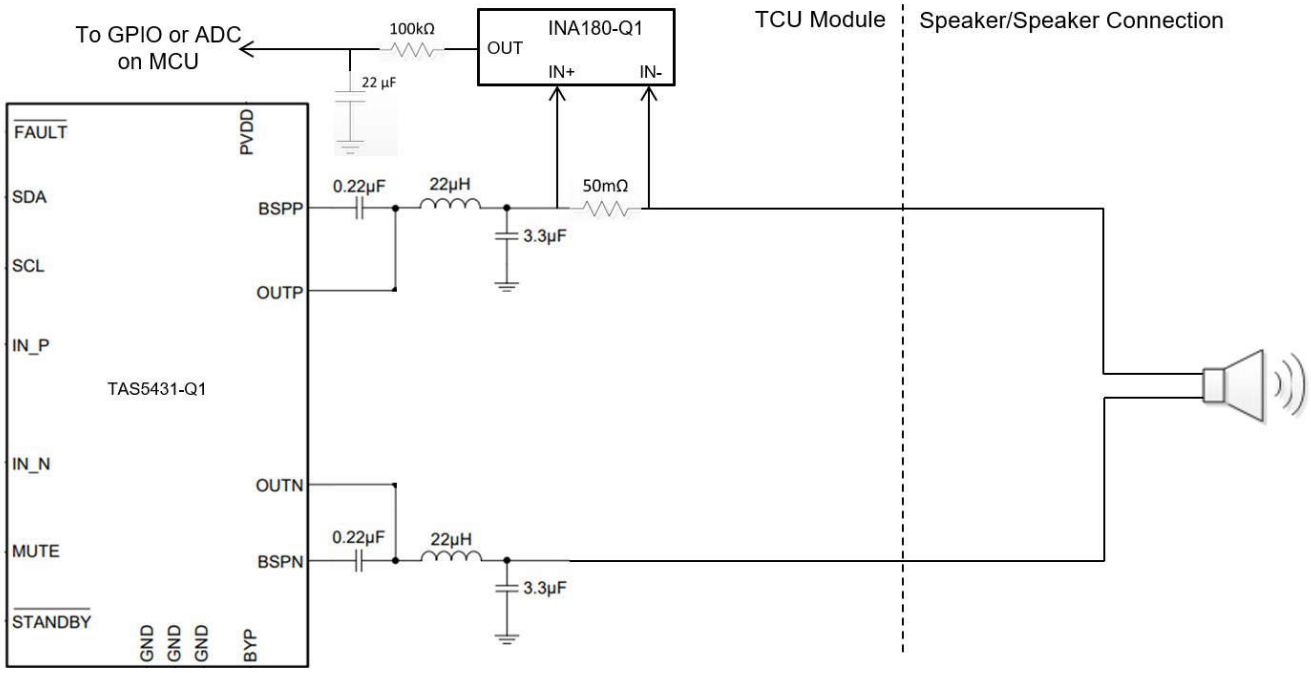

Figure 4. *Implementing a simple current-sense amplifier circuit with the TAS5431-Q1 enables the detection of open circuits*

The baseline signal generates current through the 50mΩ current-sense resistor, regardless of whether audio is present, which the **INA180-Q1** converts to a proportional voltage. Although the baseline signal is bipolar (goes both positive and negative), the unidirectional nature of the **INA180-Q1** automatically half-wave-rectifies the output voltage and vastly reduces the post-filtering requirements to a simple RC filter. The resulting DC output from the RC filter is driven into a microcontroller general-purpose input/output or analog-to-digital converter (ADC) for analysis (**Figure 5**). During an open-load failure, current will cease to flow through the current-sense resistor, forcing the output of the **INA180-Q1** to 0 V. The **INA180-Q1** output crossing a pre-determined threshold triggers an alert to disconnect the speaker (**Figure 6**).

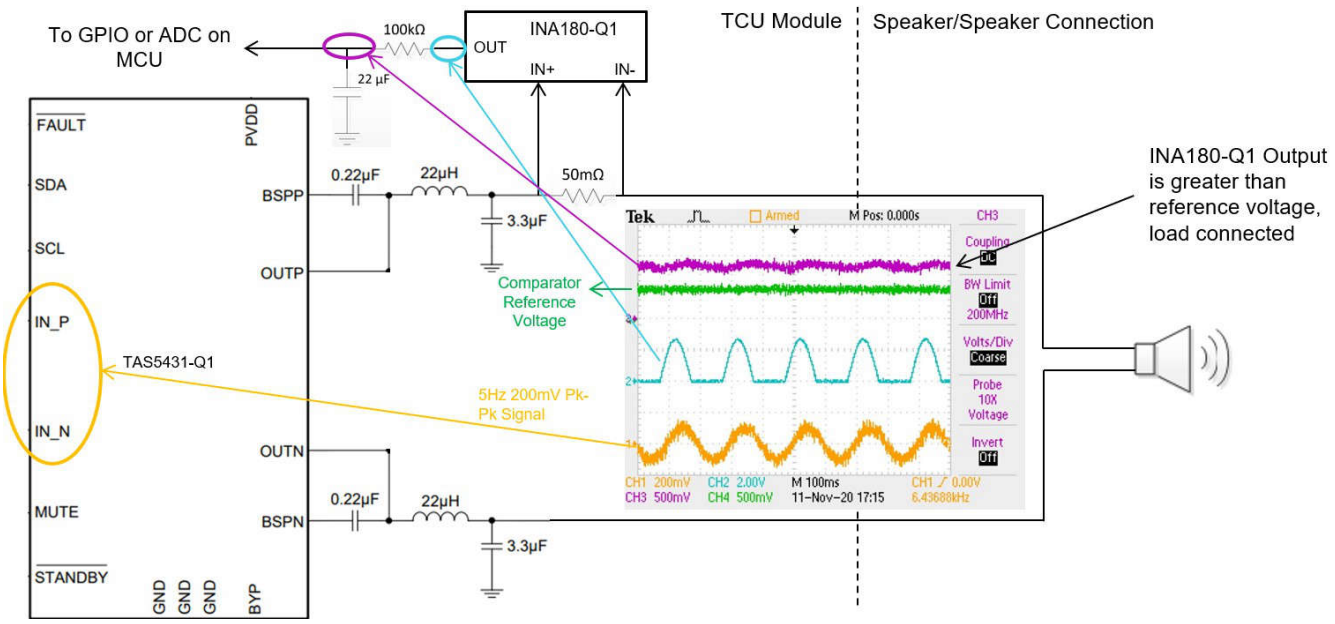

Figure 5. *During normal operation, the INA180-Q1 rectifies the baseline signal to a measurable DC voltage*

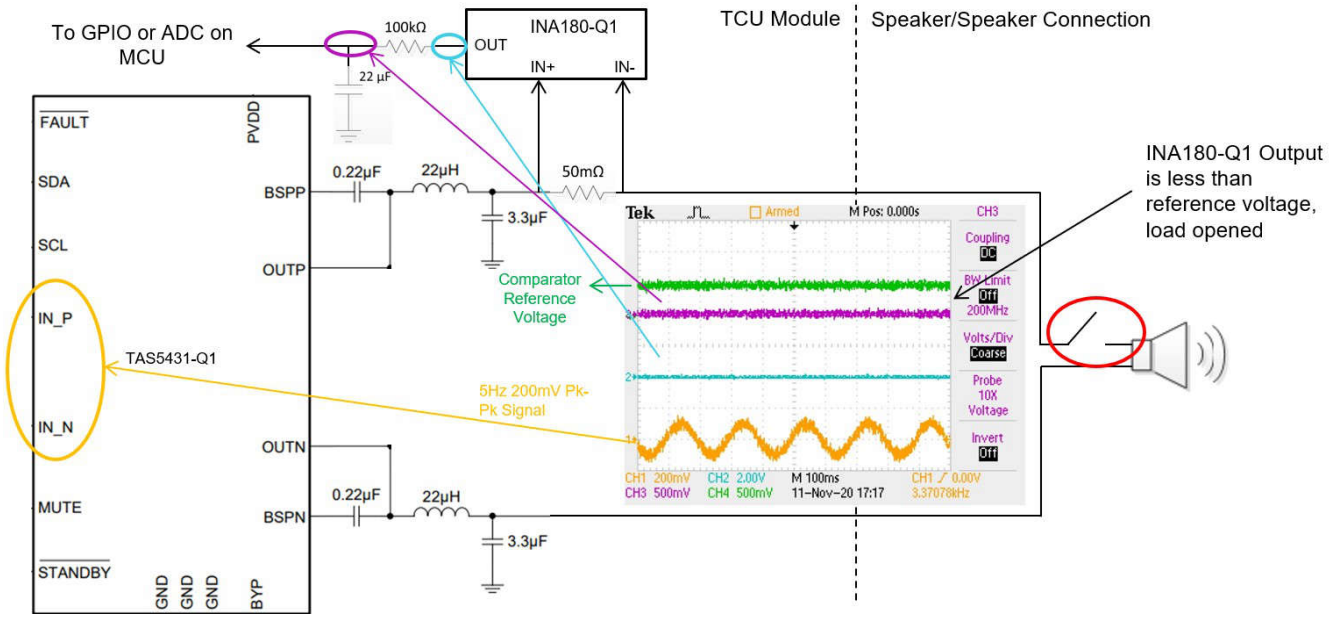

Figure 6. *During an open-fault condition, the INA180-Q1 measures zero current, which is easily detectable by an attached comparator or ADC*

Final verification of the circuit (**Figure 7**) with audio superimposed on the baseline signal yields the intended results during normal operation. The **INA180-Q1** converts load current traveling through a 50mΩ resistor to a half-wave-rectified voltage. The post-filtered result is a DC voltage of 1V, which is greater than the pre-selected threshold. All designs must be tuned to the intended load characteristics and the **INA180-Q1** is available in several additional gain options. The **INA180-Q1** also features a large common-mode input voltage range (26 V), ensuring that no damage will occur during a shorted battery fault, which typically induces up to 16 V on the lines.

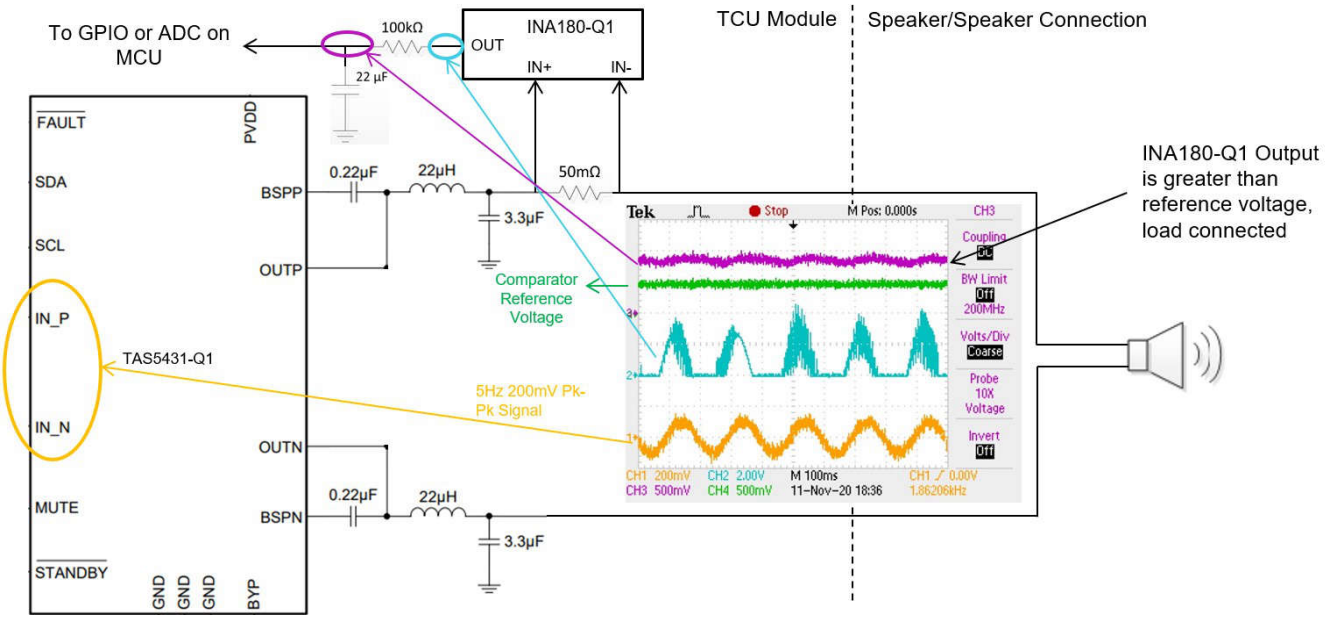

Figure 7. *Open-load diagnostics, no fault condition, audio mixed into input*

With the additional circuitry, the TAS5431-Q1 is finally able to achieve full RTD, as shown in Table 3.

	Deassertion of standby mode	Device in operation (no audio)	Device in operation (audio playing)
Positive or negative output shorted to ground	Yes	Yes	Yes
Positive or negative output shorted to battery	Yes	Yes	Yes
Positive output to a negative output	Yes	Yes	Yes
Open load	Yes	Yes	Yes

Table 3. *Summary of TAS5431-Q1 RTD when adding a baseline 5Hz 200mV peak-to-peak sine wave and additional circuitry to the Class-D input*

Additional considerations

Having achieved RTD with the **TAS5431-Q1**, there are two additional design considerations to review. The first is fault recovery. When a fault scenario is active, the Class-D amplifier should protect itself and any connected circuitry from damage, while also diagnosing the fault. Once the fault is removed, the device is expected to immediately detect that the fault has been removed and continue to play audio (if audio is being applied to the input). The **TAS5431-Q1** achieves fault recovery by continuously running its 229ms diagnostic cycle on repeat indefinitely. When a fault is removed, the diagnostic cycle determines that there is no longer a fault and allows the output stage to operate as normal. More details on this can be found in Section 7.3.5.1, "Load Diagnostics Sequence," of the **TAS5431-Q1** datasheet. The additional circuitry required to achieve RTD does not impact the device's ability to recover from a fault and immediately play audio.

The second consideration is that, depending upon the total impedance of the load, the Class-D amplifier may have difficulty detecting the positive and negative output shorted condition. Each Class-D amplifier has an impedance threshold at which it will detect the positive output and negative output shorted together (a shorted speaker). In a given design, there may be a significant amount of impedance between the positive and negative outputs, especially when a short occurs close to a speaker, which can exceed the detection threshold of the Class-D amplifier. In vehicle systems, the cabling from

the TCU module to the speaker (and back to the TCU module) can be as long as 10 to 12 meters. Figure 8 shows all the different impedances to consider.

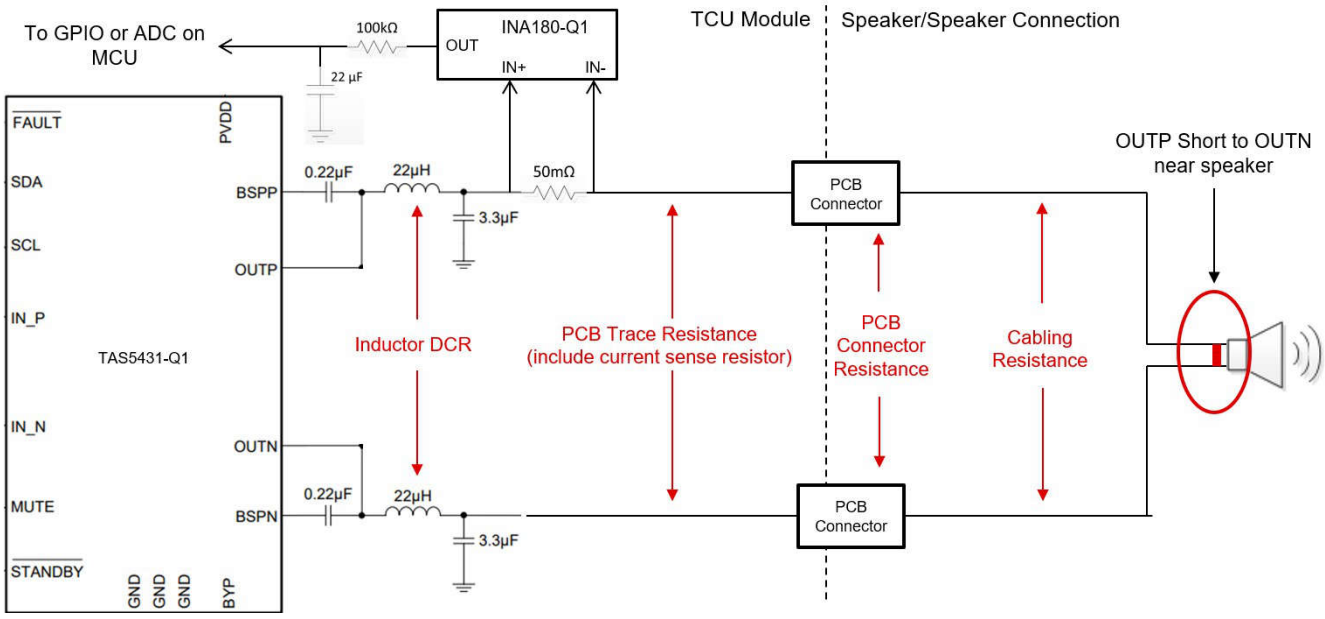

Figure 8. *Accounting for impedances between the positive and negative outputs when a positive output short to the negative output occurs near the speaker*

Next, we will review an example analysis of how to consider the various impedances in the system and compare them to the **TAS5431-Q1** detection threshold.

We can start by assuming 12 meters of 22AWG external cabling (0.053Ω/meter) totals 636mΩ of resistance, as shown in Equation 1:

$$12\,meters \times \frac{0.053\,\Omega}{meter} = 636m\Omega \quad (1)$$

Standard automotive connectors such as the Molex 34826-8160 specify approximately 20mΩ per connector, totaling 40mΩ for the two connectors.

For the inductors, it is important to find an automotive-grade, low direct current resistance (DCR) inductor such as the VAMV1009AA-220MM2 from Cyntec. The 22µH inductor has a maximum of 56mΩ, multiplied by 2 for each coil, totaling 112mΩ.

Finally, adding the 50mΩ for the current-sense resistor totals approximately 838mΩ of resistance between the positive and negative outputs, not including trace resistance.

According to the **TAS5431-Q1** data sheet, the short-circuit detection threshold specification is 900 mΩ. Thus, to ensure the device identifies a short between the positive and negative outputs, the resistance between the two must be less than 900 mΩ. Based on the total calculated 838 mΩ of resistance, there is approximately 62 mΩ of trace impedance before the **TAS5431-Q1** may be susceptible to missing a short between the outputs.

Meeting the 900mΩ specification requires careful printed circuit board design and trace routing. You can also fine-tune other aspects of the design, such as using the "**LC Filter Design**" application report to select an alternative, lower-DCR inductor, or minimize the current-sense resistor value and select an **INA180-Q1** with a larger gain setting.

Conclusion

RTD has become a critical safety aspect for TCU systems. Through a series of clever circuit design techniques, vehicle manufacturers can overcome this challenge and start implementing RTD in TCU modules today. Additional diagnostics will lead to safer vehicles and safer vehicles will lead to a better experience for all drivers on the long road ahead.

IMPORTANT NOTICE AND DISCLAIMER

TI PROVIDES TECHNICAL AND RELIABILITY DATA (INCLUDING DATASHEETS), DESIGN RESOURCES (INCLUDING REFERENCE DESIGNS), APPLICATION OR OTHER DESIGN ADVICE, WEB TOOLS, SAFETY INFORMATION, AND OTHER RESOURCES “AS IS” AND WITH ALL FAULTS, AND DISCLAIMS ALL WARRANTIES, EXPRESS AND IMPLIED, INCLUDING WITHOUT LIMITATION ANY IMPLIED WARRANTIES OF MERCHANTABILITY, FITNESS FOR A PARTICULAR PURPOSE OR NON-INFRINGEMENT OF THIRD PARTY INTELLECTUAL PROPERTY RIGHTS.

These resources are intended for skilled developers designing with TI products. You are solely responsible for (1) selecting the appropriate TI products for your application, (2) designing, validating and testing your application, and (3) ensuring your application meets applicable standards, and any other safety, security, regulatory or other requirements.

These resources are subject to change without notice. TI grants you permission to use these resources only for development of an application that uses the TI products described in the resource. Other reproduction and display of these resources is prohibited. No license is granted to any other TI intellectual property right or to any third party intellectual property right. TI disclaims responsibility for, and you fully indemnify TI and its representatives against any claims, damages, costs, losses, and liabilities arising out of your use of these resources.

TI’s products are provided subject to TI’s Terms of Sale, TI’s General Quality Guidelines, or other applicable terms available either on ti.com or provided in conjunction with such TI products. TI’s provision of these resources does not expand or otherwise alter TI’s applicable warranties or warranty disclaimers for TI products. Unless TI explicitly designates a product as custom or customer-specified, TI products are standard, catalog, general purpose devices.

TI objects to and rejects any additional or different terms you may propose.

Last updated 10/2025